



Case study

Advanced processing of high Ca fly ash for enhanced reactivity and improved high value-added application possibilities

Mária Ambrus^{*}, Gábor Mucsi*Institute of Raw Material Preparation and Environmental Processing, University of Miskolc, Miskolc-Egyetemváros, Hungary*

ARTICLE INFO

Keywords:

Fly ash
Geopolymerization
Mechanical activation
Planetary mill
Waste processing

ABSTRACT

The main purpose of the research was to examine the processing possibilities of a low-grade high Ca fly ash (FA) to increase its future utilisation potential. Size separation via sieving and mechanical activation with the use of a planetary ball mill was examined to compare the results and complement the application of the various mechanical processes. Based on the preliminary chemical analysis, the composition of the FA below and above 32 μm showed significant variations, thus, the < 32 μm size fraction was separated and the coarse fraction was utilised due to the higher Si and Al content. After milling the coarse FA for various grinding times, the frequency distribution of the < 1 μm particles showed a considerable increase but aggregation and agglomeration were also observed after 30 min, with a 5.49 μm average particle size. The pozzolanic activity almost doubled with only 5 min grinding, reaching the optimal grinding time with the highest CaO uptake value at ~20–30 min with over 160 mg/g absorbed CaO at only 20 days. According to the FT-IR analysis of the mechanically activated samples, important structural changes took place in the FA framework. Considering the geopolymerization behaviour of the samples, applying only classification can significantly reduce the compressive strength by up to a 33% decrease. However, with the mechanical activation of the coarse fraction, an over five times increase was observed in the compressive strength with the optimal grinding time.

1. Introduction

A high percentage of the energy demand is supplied with the use of coal-fired power plants all over the world, with the use of coal making up over 35% share of electricity production for the past decades. As a result, a vast amount of by-products have to be landfilled to e.g. ponds and lagoons. One such by-product is fly ash (FA) which is removed from flue gas, typically with the use of electrostatic precipitators and fabric filters. FA has fine particle size, contains unique spherical-shaped particles (cenospheres), and possesses pozzolanic properties, making it a prominent base material or additive in many fields [1–3]. To decrease the possible environmental and health hazards associated with FA storage, such as soil and groundwater contamination, and to decrease CO₂ emissions, FA utilisation has been introduced in an increasing number of industrial sectors, taking advantage of its beneficial properties. Some of the potential areas for FA use are cement and concrete production, soil amelioration, porous ceramics production, road and embankment construction, mine filling, rare metal extraction, zeolite synthesis, anaerobic digestion, or geopolymer production [1,4–8]. Thus, besides the traditional applications, many high-value-added products can be prepared from fly ash as well.

The utilization of FA can be significantly increased by adjusting its properties, such as fineness, particle size distribution, density,

^{*} Corresponding author.

E-mail address: maria.ambrus@uni-miskolc.hu (M. Ambrus).

porosity, morphology, permeability, mineral composition or pozzolanic activity [9,10]. Some of the possible methods to improve FA reactivity can be size-fractioning, chemical activation, thermal activation or mechanical activation in various mills using different milling parameters. A planetary ball mill is a characteristic high-energy mill type that can be applied for the mechanical, mechano-chemical activation of numerous materials [9,11–14]. For planetary ball milling, several factors affect the mechanical activation process and the final properties of the ground materials, including the material properties, the rotation speed, the material and ball filling ratio, grinding time, etc. [9,15].

As a traditional utilisation method, FA after sieving [16,17], milling [18,19], and classification with dust cyclone [16] and electrostatic precipitator [20] have been examined with promising results for the cement and concrete industry, especially as fine-sized FA with a combination of other additives can significantly improve the fracture toughness and mechanical properties, compared to ordinary Portland cement-based concretes [21,22]. As a high value-added application of FA, mullite-based porous ceramics can be prepared with the use of milled, or sieved and milled FA. Using lower particle-sized FA can decrease open porosity, improve compressive and flexural strength, and lower thermal conductivity, making FA-based mullite-based porous ceramics superior to traditional ones [23,24]. For zeolite synthesis or CO₂ sequestration, a smaller particle size is required and the FA is generally ground and sieved before use [25,26]. FA rich in silicon and aluminium species can be used as a potential raw material for zeolite synthesis, while for CO₂ sequestration, high-Ca, low-Ca FA, or even a mixture of both types can be used [27,28]. Rare earth elements and yttrium (REY) can also be recovered from FA, the quantity of these elements is generally more enriched in the finer particle size fractions [29,30]. Grinding and sieving can also be integrated during catalyst synthesis from FA after the necessary thermal and chemical pre-treatments [31].

Geopolymers are novel inorganic materials which can be prepared with the use of industrial wastes and by-products, including FA as a common base material. With their advantageous properties of high mechanical strength, acid, heat and fire resistance, low shrinkage and thermal conductivity, and good adhesion to various material surfaces, many products and utilisation methods have been examined and used in the past decades. High reactive silica and alumina content are required for the geopolymerization process, while the high Ca content can have negative effects on the setting time or the resistance to certain chemicals of the final products and the high S content can result in lower geopolymer compressive strength and resistance to corrosion [32,33]. The proportion of researchers using the coarse fraction of sieved FA for geopolymerization is rather low, and the composition and the fate of the unused FA fraction are not discussed [34,35]. FA reactivity in the case of geopolymerization is highly influenced by the reactive amorphous phase content and the small particle size, as a consequence, high specific surface area. Size-fractioning of the smaller particle size fractions and mechanical activation of FA followed by sieving have already been proven to be an effective method to further improve the properties of geopolymers [36–39]. However, the examination of the separated fine fraction and the mechanical activation of the coarse fraction to determine the complex utilisation possibilities of FA is a currently unexplored research area.

The focus of the research was the combined processing of FA by sieving and mechanical activation to decrease the amount of landfilled FA. Due to the highly different chemical composition of the obtained size fractions, the coarse FA was mechanically activated to evaluate the possibility of geopolymer production. The classified and milled samples were characterised, and future utilisation possibilities were proposed based on the examined properties, such as geopolymer production.

2. Materials and methods

The raw material for the experiments was a lignite-type fly ash sample acquired from the Mátra Power Plant (Hungary). The sample was dried at 105 °C until constant mass, then the > 1 mm contaminants were removed by manual sieving.

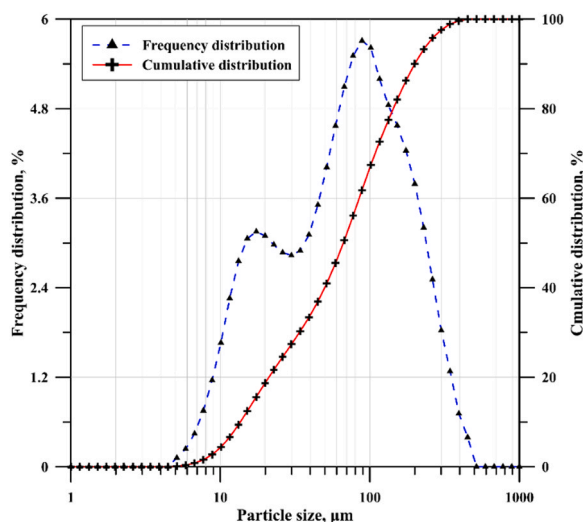


Fig. 1. Cumulative- and frequency curves of the particle size distribution.

The particle size analysis was carried out with a Horiba LA-950 V2 type laser particle size analyser in wet mode using distilled water, with the Mie-scattering theory applied to calculate the particle size / cumulative distribution and geometric surface area values. For each measurement, 1 ml of Na-pyrophosphate was added as a dispersing agent and ultrasound treatment was used to further aid the dispersion and disaggregation of particles due to the hydrophilic nature of FA. The particle size of the base FA ranges from 5 to 450 μm with a bimodal frequency distribution curve, with the two peaks located at 11 and $\sim 100 \mu\text{m}$ (Fig. 1). The geometric surface area was calculated to be $601.41 \text{ cm}^2/\text{g}$.

The particle density of the samples was measured via the pycnometer method. The specific gravity of the base FA was 1.93. The porosity (Φ) of the FA samples was calculated based on the bulk (ρ_b) and particle density (ρ_p) of the samples with the following Eq. (1) [40]:

$$\Phi = 1 - \frac{\rho_b}{\rho_p} [-] \quad (1)$$

The loss on ignition (LOI) was measured with the samples heated to 950°C with 90 min heating time, and 60 min holding time. The LOI of the base FA was 5.76%, indicating a high amount of unburned carbon content, as well as the possible reactions of carbonates, bound water and sulphur and iron-containing minerals [41].

A Rigaku Supermini 200 type wave-length X-ray fluorescence spectroscopy was used for the chemical analysis of the FA samples. The spectroscopy was equipped with a 200 W (50 kV and 4.0 mA) Pd cathode X-ray tube, using the ZSX programme. As a preliminary analysis of the FA sample, six size fractions ($>90 \mu\text{m}$, $90\text{--}63 \mu\text{m}$, $63\text{--}45 \mu\text{m}$, $45\text{--}32 \mu\text{m}$, $32\text{--}20 \mu\text{m}$, $<20 \mu\text{m}$) were prepared from the base material for chemical analysis, to examine the distribution and possible enrichment of various components in certain fractions (Table 1). The main components of the base sample are SiO_2 , Al_2O_3 , Fe_2O_3 , CaO , SO_3 and MgO , containing 46.6%, 16.2%, 9.4%, 9.39%, 5.25% and 2.96%, respectively. The desulphurization process at the power plant entailed the high calcium oxide and sulphur trioxide content of the FA. Other elements of the samples included As, Ba, Co, Cr, Cu, Ni, Pb, Rb, Sr, Zn and Zr. Based on the ASTM C618 classification, the base FA is considered Class F with a total $\text{SiO}_2 + \text{Al}_2\text{O}_3 + \text{Fe}_2\text{O}_3$ content of 72.2%. The distribution of the various components is not homogeneous in the sample. In the case of most of the examined oxides, significant composition differences can be observed, mainly below and above $32 \mu\text{m}$ particle size value, determining the particle size for the size separation of the sample. The $< 32 \mu\text{m}$ fraction made up 26.85 wt% of the sample.

The component yield of the sieved fractions (c_i) was calculated based on the component content of the base material (a), the sieved fractions (a_i) and the mass yield of the fractions (v_i) values of the sieving, using Eq. (2) [42]:

$$c_i = v_i \frac{a_i}{a} [\%] \quad (2)$$

The FT-IR spectra were measured with a JASCO FT-IR 4200 type spectrometer equipped with a single-reflection diamond ATR. During the analyses, the spectra were collected in the absorbance range from 7800.65 to 349.053 cm^{-1} , at a resolution of 4 cm^{-1} , and baseline corrected. The morphology and elemental composition of the samples were examined with Phenom ProX EDX scanning electron microscope equipped with a high-sensitivity backscattered electron detector. A Fritsch Pulverisette 5 Premium line high energy planetary mill was used for the mechanical activation experiments. The mill was equipped with two 500 ml steel bowls, 9 pieces of $\varnothing 20 \text{ mm}$ steel balls in each. The mill was operating with 400 rpm, using reverse milling cycles and 5 min pause times, with total milling times of 5, 10, 20, 30, 60 and 120 min.

The pozzolanic activity was examined based on the test method described in Hungarian standard MSZ 4706–2:1998 *Complements for cement. Natural pozzolanic complements (trass) for cement*. The method is similar to the saturated lime test [43]. For the test, 2 g of samples are put into plastic containers then 100 ml of saturated lime solution is added then sealed and shaken thoroughly. The containers are shaken every day and 50 ml of solution is removed every second day for titration with 0.05 mol/L hydrochloric acid solution using methylene orange indicator. After titration, 50 ml of fresh lime solution is added to the container. From the results, the CaO uptake of 1 g material can be calculated.

For geopolymer production, 8 M NaOH solution was used as an alkaline activator. After mixing, the pastes were put in

Table 1
Chemical composition of the analysed FA fractions.

	Base sample	$x > 90 \mu\text{m}$	$63\text{--}90 \mu\text{m}$	$63\text{--}45 \mu\text{m}$	$45\text{--}32 \mu\text{m}$	$32\text{--}20 \mu\text{m}$	$20 \mu\text{m} > x$
SiO_2	46.6	54.7	49.7	49.0	47.7	41.7	37.1
Al_2O_3	16.2	19.4	17.2	17.2	16.5	13.9	12.6
MgO	2.96	2.51	2.89	2.99	3.13	3.20	3.81
CaO	9.39	6.87	8.41	8.31	8.77	11.0	14.5
Na_2O	0.50	0.48	0.47	0.49	0.51	0.47	0.58
K_2O	1.64	1.65	1.66	1.71	1.73	1.58	1.57
Fe_2O_3	9.4	8.1	8.9	9.1	10.2	13.3	13.3
MnO	0.147	0.095	0.132	0.142	0.154	0.173	0.208
TiO_2	0.549	0.612	0.566	0.588	0.580	0.506	0.435
P_2O_5	0.270	0.162	0.231	0.254	0.284	0.330	0.433
SO_3	5.25	2.25	3.9	3.15	3.3	6.75	11.1
F	< 0.3	< 0.3	< 0.3	< 0.3	< 0.3	< 0.3	< 0.3
Σ	92.91	96.83	94.06	92.93	92.86	92.91	95.64

20 × 20 × 20 mm cubic moulds, and heat treated at 60 °C for 6 h. The uniaxial compressive strength tests were carried out on 5 specimens for each mixture, after 7 days. Some of the geopolymer specimens in the mould can be seen in Fig. 2.

3. Results

3.1. FA classification

3.1.1. Component yield

Based on the chemical composition of the sieved samples, the sum of SiO₂, Al₂O₃, and Fe₂O₃ content of the coarse fraction was 72.49%, while for the fine fraction, the sum of SiO₂, Al₂O₃ and Fe₂O₃ was 65.95%. Thus, similarly to the base FA, the coarse fraction is considered Class F but the fine fraction can be regarded as Class C FA. The LOI of the fine fraction increased compared to the base FA and the coarse fraction, implying the possible enrichment of unburned carbon, carbonates, and/or sulphur- and iron-rich minerals. Table 2.

The calculation of the component yields revealed that all components are enriched in the coarse FA fraction, with the highest values including the Al₂O₃, SiO₂, TiO₂ and K₂O reaching over 70%. In the fine fraction, no enrichment can be observed but the highest component yields of over 30% were calculated for the P₂O₅, Fe₂O₃, CaO, Na₂O, MnO and SO₃. However, because of the overall low quantity of the P₂O₅, Na₂O and MnO in the base material (Table 1), the Fe₂O₃, CaO and SO₃ content are the most dominant in the fine FA.

3.1.2. Structural characterisation by FT-IR analysis

Using FT-IR spectroscopy, the base FA and both separated fractions were examined (Fig. 3). The bands at ~1617 cm⁻¹ represent the H–O–H bending vibrations of a small amount of molecular water in the case of all three spectra. The peaks around 1400–1440 and ~872 cm⁻¹ are the indication of C–O stretching and bending of carbonates, such as CaCO₃. The intensity of this band was the highest for the < 0.032 mm fractioned FA and the lowest for the coarse FA spectrum. Thus, the carbonates are enriched in the separated, finer size fraction. Carbonate species are formed via the atmospheric carbonation of the possible Ca(OH)₂ content of the sample which in turn could be used for the indirect estimation of the CaO content [44]. At ~950–1200 cm⁻¹ wavenumber, the characteristic peaks of the TO₄ tetrahedra (T = Al, Si) are found, which can also help with the identification of the crystalline and amorphous phases. The bands at ~1007 cm⁻¹ are characteristic of the stretching vibrations of Si–O or Al–O bonds of silicates, ~1087 cm⁻¹ for the quartz, and ~1141 cm⁻¹ for mainly quartz and mullite. The sharp bands appearing at 660 and 597 cm⁻¹ are generally the indication of Ca-sulphides, such as anhydrite, gypsum or bassanite in the sample [45]. Other bands related to the probable sulphate groups are not detectable due to the co-occurrence with the characteristic peaks of the TO₄ tetrahedra [44,46–48]. In the spectrum for the coarse sample, the intensity for the quartz decreased and there was a significant increase for the amorphous phase. On the other hand, the intensities of the carbonate and observable sulphate bands were significantly higher in the finer particle size fraction. Thus, the

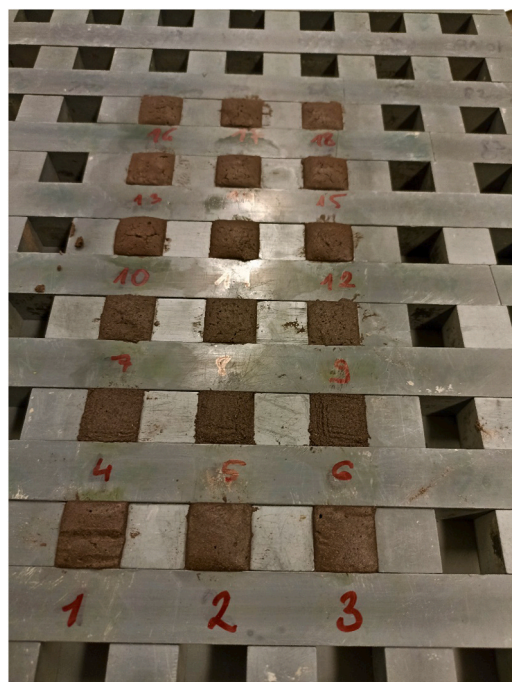


Fig. 2. Geopolymer specimens in the mould.

Table 2
The component yield and LOI of the classified samples.

Component, %	Coarse	Fine
SiO_2	76.59	23.41
Al_2O_3	77.15	22.85
MgO	69.17	30.83
CaO	67.64	32.36
Na_2O	68.71	31.29
K_2O	73.38	26.62
Fe_2O_3	63.77	36.23
MnO	65.23	34.77
TiO_2	75.36	24.64
P_2O_5	62.22	37.78
SO_3	65.81	34.19
LOI, %	5.65	6.15

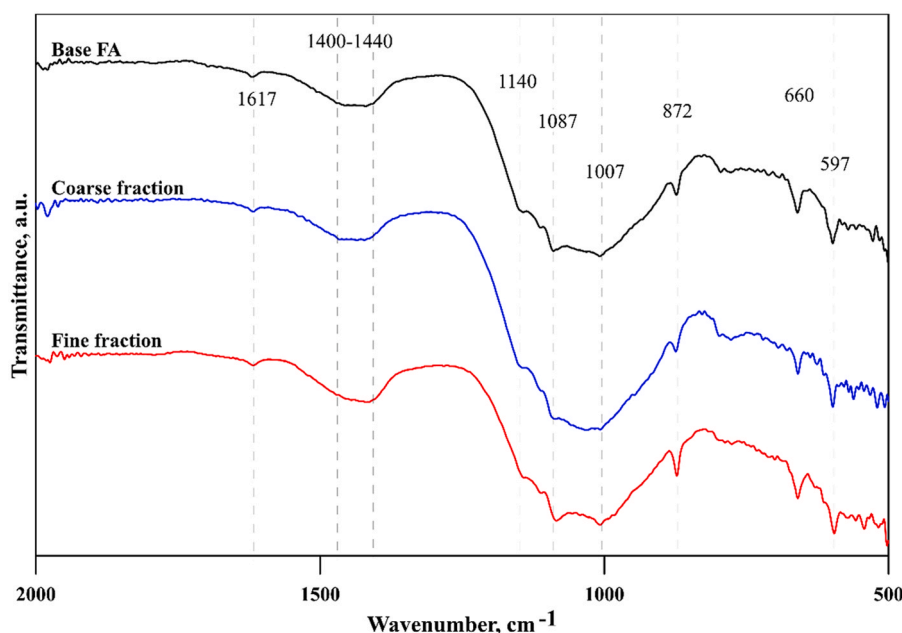


Fig. 3. FT-IR spectra of the base and classified FA samples.

comparison of the FT-IR spectra with the chemical analysis reveals a good correlation between the data.

3.1.3. SEM and EDS analysis

With SEM analysis, both the morphology of the FA and the characterisation of the potential mineral phases are possible. The base FA contains many spherical and irregularly shaped particles, and different mineral aggregates (Fig. 4.a). The morphology of the FA particles is influenced by several factors, such as the chemical composition and the various states of the elements, i.e. Si, in the FA, the cooling of the flue gas, and the temperature and combustion parameters of the coal [49,50].

The typically smooth spherical particles indicate the high Si content of the sample, and these are predominantly glassy [49,51]. The EDS analysis at Point 1 revealed that the main elements composing the porous aggregate particle are O, Si, and Al, with a small amount of Na, K, Ca and Mg as trace elements, implying that the larger fused particles are various silicate phases. The generally spherical bright particles with rough, irregular surfaces at Point 2 were found to be iron oxides, such as hematite, magnetite or maghemite that are common mineral constituents of FAs. The similarly bright, dendritic structured particles are assumed to have the same iron-rich composition. The analysis of the more angular particle at Point 3 revealed that it was composed of O, Ca and S, suggesting the sulphate phases also seen in the FT-IR spectra.

The comparison of the images of the coarse and fine FA fractions (Fig. 4.b and c) shows the significant difference in the particle sizes of the samples. A high amount of aggregated particles can be found in the coarse fraction, along with a smaller quantity of spherical particles and iron-rich and sulphate-containing particles. On the other hand, the number of angular sulphates, iron oxides and smooth spherical glassy particles are considerably higher in the fine fraction.

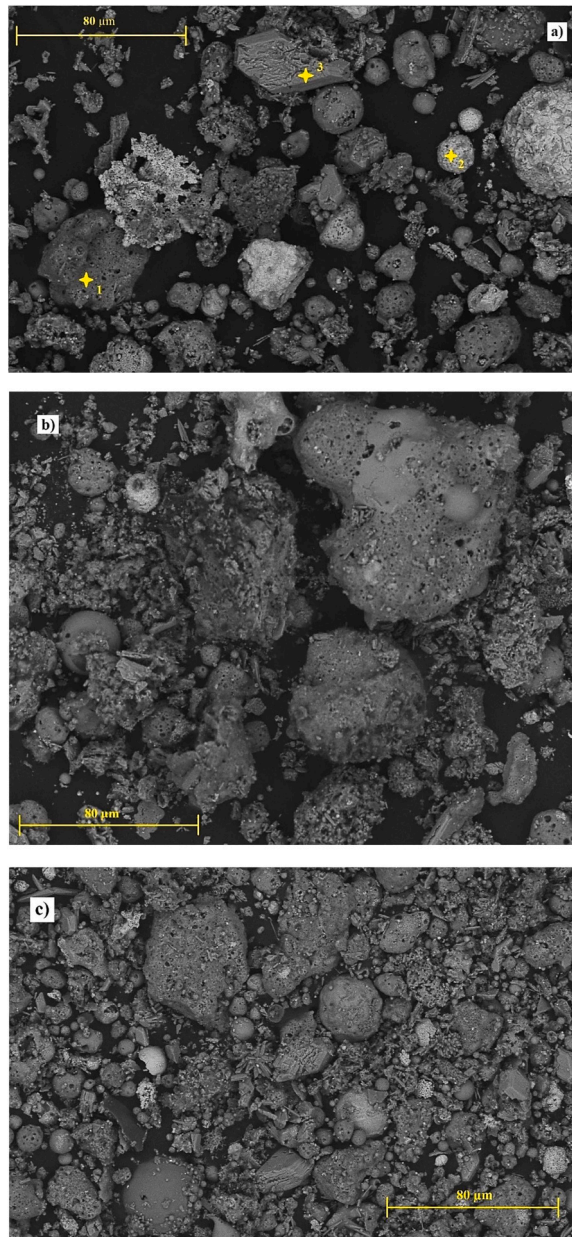


Fig. 4. SEM images of the (a) base, (b) classified coarse and (c) fine FAs at $900\times$ magnifications.

3.1.4. Geopolymerization behaviour

After the removal of the fine particle fraction, the geopolymerization behaviour of the base FA and the silica- and alumina-rich coarse fraction was examined with different liquid-to-solid ratios (1.22, 1 and 0.82) which influenced the $\text{SiO}_2 / \text{Na}_2\text{O}$ and $\text{Na}_2\text{O} / \text{Al}_2\text{O}_3$ ratios of the mixtures (Fig. 5.). The $\text{SiO}_2 / \text{Na}_2\text{O}$ ratios changed between 1.95 and 2.99, and the $\text{Na}_2\text{O} / \text{Al}_2\text{O}_3$ ratios varied between 1.68 and 2.65.

With the changes in the $\text{SiO}_2 / \text{Na}_2\text{O}$ ratio of the mixtures, the coarse FA-based geopolymers showed a linear decrease in the uniaxial compressive strength, while the base FA geopolymers had an initial $\sim 12\%$ increase before a sharp incline. Regarding the $\text{Na}_2\text{O} / \text{Al}_2\text{O}_3$ ratios, increasing the ratio led to higher compressive strength values, achieving almost 200% better results with the coarse FA geopolymers.

Considering not only the compressive strength but the workability of the pastes and the expected improvement due to mechanical activation, a 1 liquid-to-solid ratio was applied for the subsequent geopolymer production. This corresponded to 2.45 and 2.05 $\text{SiO}_2 / \text{Na}_2\text{O}$ and $\text{Na}_2\text{O} / \text{Al}_2\text{O}_3$ ratios, respectively.

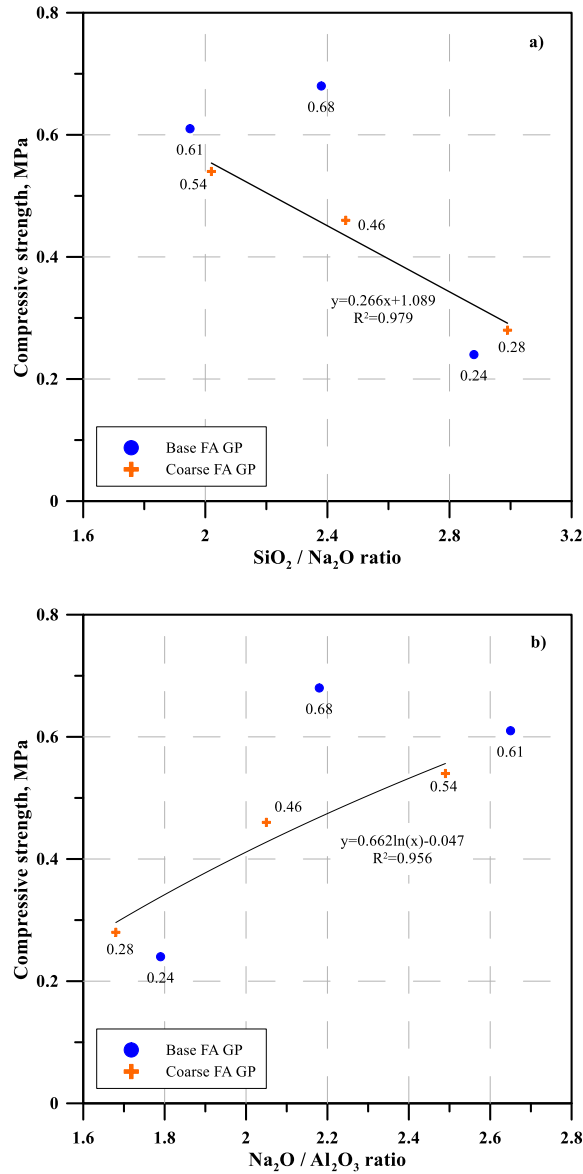


Fig. 5. UCS of the geopolymer specimens with different a) $\text{SiO}_2 / \text{Na}_2\text{O}$ and b) $\text{Na}_2\text{O} / \text{Al}_2\text{O}_3$ ratios.

3.2. Mechanical activation

3.2.1. Physical properties

Generally, the changes in the geometric surface area in relation to the grinding time in the planetary mill followed a logarithmic trend (Fig. 6). The calculated geometric surface area considerably increased with a longer grinding time. After 60 min and $30877 \text{ cm}^2/\text{g}$, the flattening of the surface area curve was observed, the surface area reaching up to $32921 \text{ cm}^2/\text{g}$ with 120 min. However, the total increase was over $8 \times$ higher than the $4036.89 \text{ cm}^2/\text{g}$ achieved by using 5 min grinding.

The characteristic particle sizes (x_{10} , x_{50} and x_{90}) in relation to the geometric surface area values and the particle volume distributions of the ground samples are illustrated in Fig. 6. The reactivity of FA is highly affected by its fineness [20]. Regarding the frequency distributions of the samples seen in Fig. 7.a, the original bimodal curves of the 5–30 min ground samples had a sharp increase in the intensity of the first, $< 1 \mu\text{m}$ mode which reached considerably higher value after 60 and 120 min milling. A decrease in intensity and a shift to a smaller particle size from $11 \mu\text{m}$ to $4 \mu\text{m}$ was seen in the second mode of the frequency distribution curves. After 60 min, a third and fourth mode also appeared in the ~ 100 and $110 \mu\text{m}$ particle size region. With 120 min grinding, the fourth mode disappeared, and the third mode shifted to $\sim 50 \mu\text{m}$.

Considering the characteristic particle sizes of the ground FAs (Fig. 7.b), with the increasing geometric surface area and grinding time, the x_{10} and x_{50} particle sizes continuously decreased, stagnating after 60 min. At 120 min grinding, the median (x_{50}) particle size

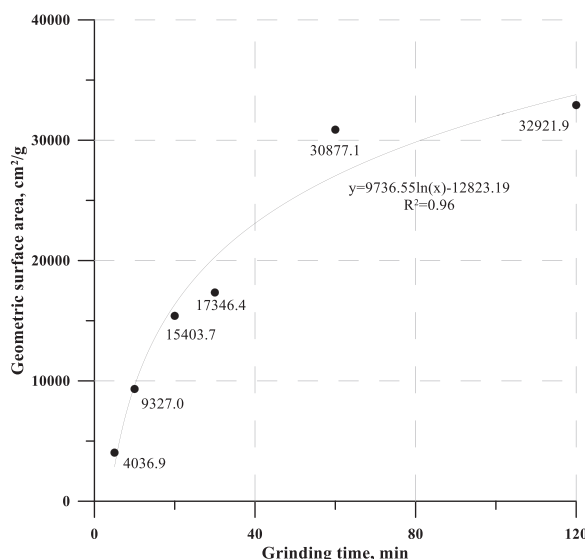


Fig. 6. The geometric surface area of the ground FAs.

decreased by 75% and the x_{10} value by over 93%. The x_{90} particle size had a rapid decrease of ~50% but after reaching 15400 cm²/g (20 min grinding), the values started increasing from 18.86 μ m to 28.33 μ m, resulting in a 50% increase from 20 min to 120 min grinding time. Thus, even though the geometric surface area was increasing with the grinding, the aggregation of the FA could be observed after 20 min grinding in the planetary mill. On the other hand, the smallest measured particle size reached 0.1 μ m with 20 and 30 min milling and was further reduced below 0.1 μ m using longer grinding times.

The specific gravity of FA depends mainly on the particle shape, size distribution and the coal type used for combustion [52]. The specific gravity (Table 3) increased by over 30% after only 5 min grinding compared to the coarse sample due to the production of fine particle size fraction that was previously removed via classification. The values plateau between 10 and 30 min and increase again after 60 min, reaching a stable 2.51 with the additional prolonged grinding till 120 min. However, as the specific gravity change after 30 and 60 min milling is only ~3%, it can be concluded that the low specific gravity constituents of the FA, such as plerospheres and hollow cenospheres, were mostly crushed after approximately 20–30 min of planetary milling [53].

3.2.2. Pozzolan activity

As a traditional utilisation method, FA can be applied as a base material for hydraulic binder production or as a cement substitute in concrete structures due to its pozzolanic character, as it tends to improve the compressive strength of cementitious composites [54]. Various physical methods can be used to improve the pozzolanic activity of FA, like classification, grinding or mechanical activation. During the experiments, the pozzolanic activity test could not be completed for the FAs with 20–120 min grinding due to the significant swelling of the material in the saturated lime solution (Fig. 8.a). In Fig. 8.b, the CaO uptakes of the samples at each titration test are illustrated, displaying the values until the 20th day (10th titration) for the 20–120 min ground samples.

The removal of the fine fraction resulted in only a slight decrease in the total CaO uptake, which decreased from 116.3 to 111.3 mg/g FA. With only 5 min grinding of the coarse FA, the total CaO uptake of the sample more than doubled, in relation to both the base and the coarse sample.

In comparison with FA ball milling experiments described by Mucsi and Csöke (2014), using the same standard to examine the pozzolanic reactivity, planetary milling results in considerably higher CaO uptake than ball milling. The highest adsorbed CaO after the ball milling of various FA samples was 173 mg/g, with the surface area of the samples reaching ~6300 cm²/g [55]. The planetary milling of FA for only 5 mins resulted in a lower surface area than the reported ball milling values, only 4036.9 g/cm², however, the adsorbed CaO was 217.8 mg/g for the sample. Thus, indicating that prolonged grinding times in a ball mill could be substituted by shorter planetary milling to sufficiently increase the pozzolanic reactivity of FAs.

Comparing the 20-day values of all the planetary milled samples, the CaO uptake got higher until the grinding time reached 20–30 min but slightly decreased with 60 and 120 min milling, indicating that the pozzolanic activity was increased by the mechanical activation. However, the extended planetary milling of the FA resulted in reduced values. In the case of the analysed FAs, 20 min grinding in a planetary ball mill is a preferably short milling time to sufficiently increase the pozzolanic activity and surface area, and to decrease the particle size of FA for further use.

3.2.3. Structural characterisation by FT-IR analysis

The effect of prolonged mechanical activation can be seen in all of the examined peaks in the FT-IR spectra in Fig. 9. The band at ~1600 cm⁻¹ suggesting the water content of the FA completely disappeared from the spectra after 60 min grinding. Heat production during high-energy dry grinding is a commonly observed phenomenon that can also be an issue for certain material types, leading to

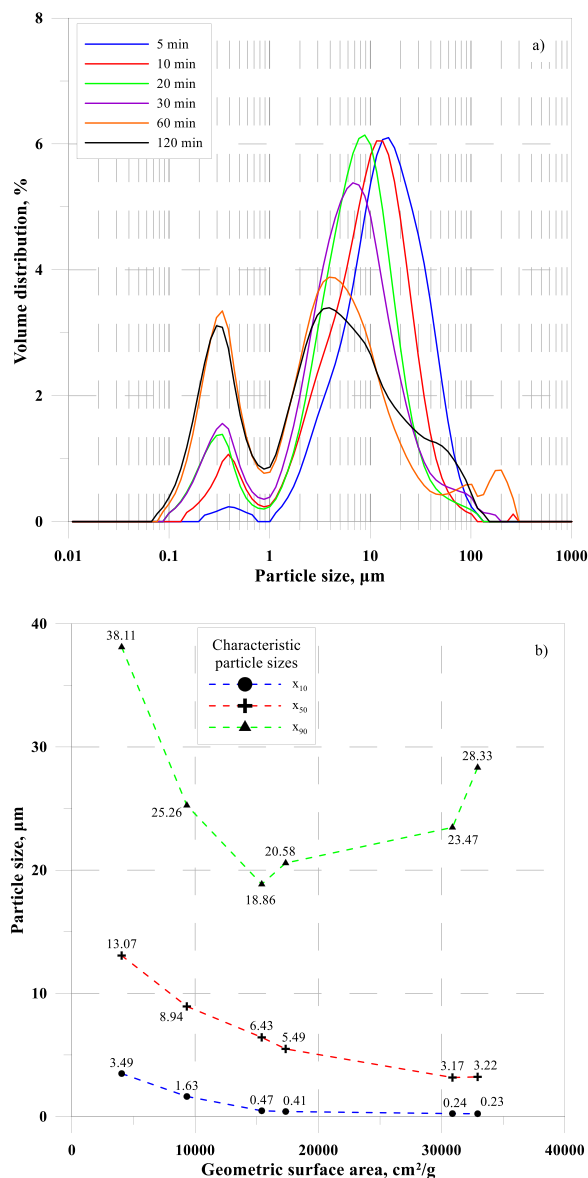


Fig. 7. The frequency distribution values (a) and characteristic particle sizes (b) of the ground FAs.

Table 3

The changes in the specific gravity and porosity values of the particles.

Grinding time, min	0	5	10	20	30	60	120
Specific gravity	1.76	2.36	2.41	2.43	2.43	2.51	2.51
Φ	0.65	0.77	0.80	0.79	0.78	0.74	0.73

the overheating of the sample [56]. Even though overheating was not a concern for FA grinding, the temperature increase of the samples after 60 and 120 min milling was noticeable during the research, which could explain the evaporation of the remaining water content of the FA sample. Also, the bands of the Ca-sulphides of 660 and 597 cm^{-1} progressively disappeared with the mechanical activation, and the peaks are not detectable after 60 and 120 min

The band corresponding to the Si–O or Al–O bonds in the silicate phases increased in intensity, broadened and the peak shifted to a higher wavenumber, to $\sim 1150 \text{ cm}^{-1}$ during mechanical activation, especially after 20 min or longer grinding. Peak intensity is highly affected by the surface area of the particles, while the change in the wavenumber can be explained by the sensitivity of the stretching modes to the Si/Al ratio of the system. Thus, if the peak shifts to a higher value, it indicates the recrystallisation of the silicate

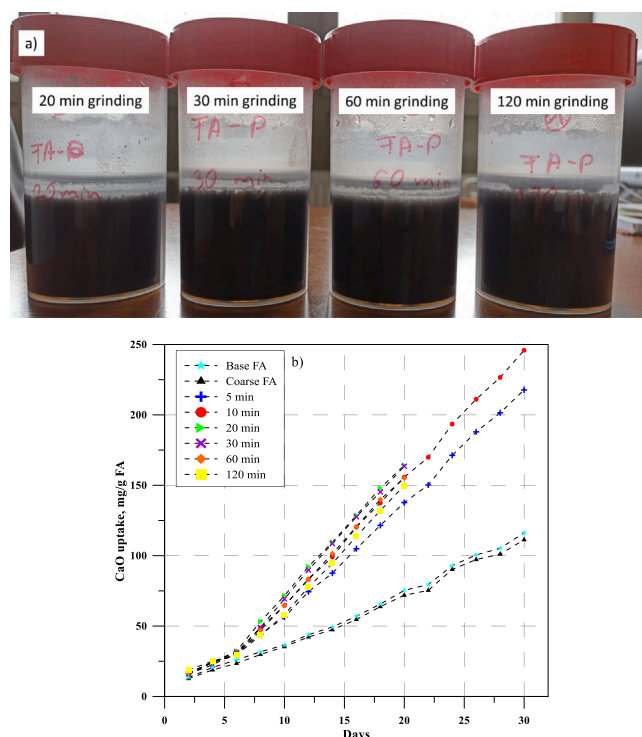


Fig. 8. a) The swelling of the 20–120 min ground samples and b) the CaO uptake of samples during the pozzolanic activity test.

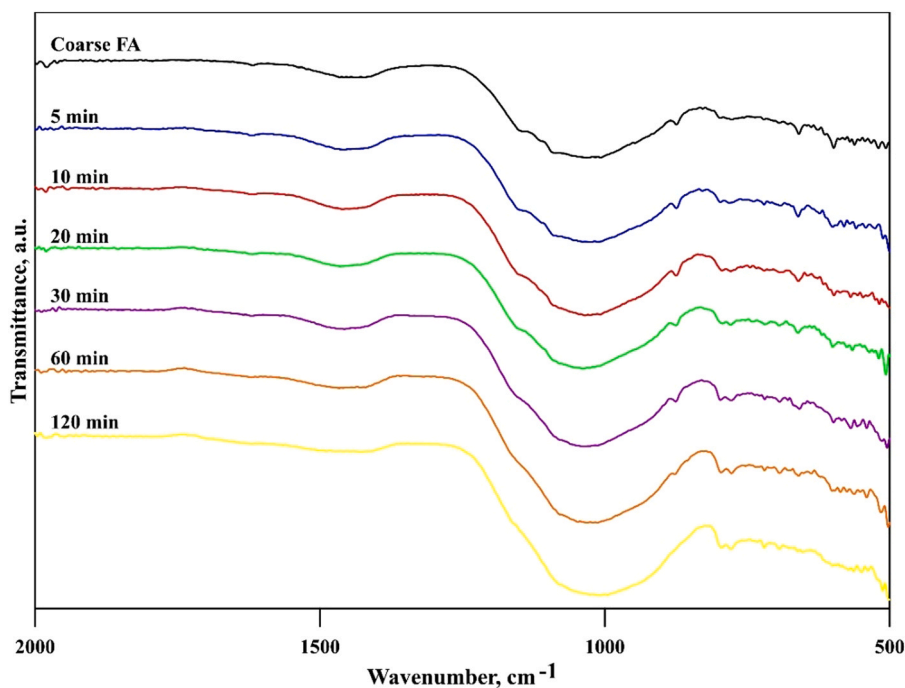


Fig. 9. The FT-IR spectra of the mechanically activated FAs.

structures, as the length of the silicate chain increases [57,58].

The continuous intensity-increase of the double peaks at 794 and 778 cm⁻¹ that are characteristic of quartz can be observed with longer grinding times. While in the coarse sample, these appear as one singular broad peak, the separation of the two peaks already

starts at 5 min, and finally, both prominent peaks appear after 30 min. The explanation of such behaviour might be the breakdown of the covalent bond in the silicate network of FA, and the availability of non-bridging oxygen for partial recrystallisation or polycondensation [51,59]. The increasing wavenumber for silicate bonds and stronger intensity of quartz peaks were also observed during the mechanical activation of volcanic ash samples. With the volcanic ash FT-IR results substantiated with XRD analysis, the higher presence of quartz in the ground samples was confirmed. However, this quartz can have positive effects, as it can act as a micro-aggregate reinforcing the structure, decreasing the water absorption of geopolymer matrices [59].

3.2.4. Geopolymerization behaviour

The uniaxial compressive strength and specimen density of the ground FA geopolymer samples were examined (Fig. 10). As expected, only 5 min high energy grinding already improved the mechanical properties of the specimens, almost doubling the compressive strength. The strength values showed a linear increase until 20 min grinding, peaking at 2.35 MPa, which is over five times higher than for the non-ground sample. With longer grinding times, the compressive strength gradually decreased, mirroring the trend of the x_{90} values seen in Fig. 7.b.

The specimen density values increased with up to 20 min grinding time, similarly to the strength values. However, using longer grinding times had no significant effect on the densities of the geopolymer samples. Based on the results, it can be concluded that the specific gravity and porosity changes in the mechanically activated FA had no substantial impact on the density of the specimens after the 1.39 g/cm³ value was achieved.

4. Discussion

4.1. Size separation

The fly ash used for the research was a lignite type, low-grade FA, the use of which is rarely examined, despite its huge potential [60]. The composition difference between the coarse and fine fractions presumes the feasibility of different utilisation possibilities of the two fractions after classification. The pozzolanic property of Class F (like the examined coarse) FA is generally higher as compared to Class C (the examined fine) FA, but Class C fly ash showed better performance than Class F during tests for pavement subgrade stabilisation [52,61]. Similarly, the comparison of high and low lime FAs sieved to various particle sizes revealed that the high lime FA with the smallest particle size had better performance and yielded higher compressive strength values in Portland cement – FA mortars [17]. Furthermore, fine FA tends to reduce the water requirement of mortar mixes [16]. As the LOI of the finer fraction was also higher, applications not influenced by the LOI value are also feasible, such as structural or flowable fill, or asphalt filler [52].

In the fine FA, the quartz content is higher according to the FT-IR analysis, which is a necessary source of silicon for zeolite formation. However, high-Ca FA is not ordinarily used for zeolite synthesis [62,63]. Regarding mullite production, even though the size interval would be favourable, the composition, especially the high Ca and S species and the relatively low silica and alumina content would negatively affect the products [24]. On the other hand, high-calcium FA has been proven to be successfully applicable for CO₂ sequestration in the past through accelerated carbonation reaction [28,64].

The untreated (not mechanically activated) FA geopolymers had relatively low uniaxial compressive strength values, which can be explained by the low surface area due to the large particle size. It was observed that the base FA had generally higher compressive strength values, which was to be expected due to the removal of the fine aluminosilicate and silicate particles, along with the characteristic cenospheres of FA via sieving.

4.2. Mechanical activation

In the case of high-energy dry grinding processes, such as planetary milling, the aggregation and agglomeration of particles have been reported in the case of various different materials [12,65–67]. At the start of the examined grinding process, the rate of particle size reduction was high and slowed down after 20 min as a general characteristic transition from the Rittinger stage to the aggregation stage during grinding. Based on the theory behind grinding kinetics [38,68], as a part of the aggregation stage, the adhesion of the ground particles to the surface of the grinding media and chamber is a typical behaviour which was also observed with milling times over 20 min. Most frequently the changes in median (x_{50}) particle size and surface area are reported in relation to the stages of grinding, thus, the classified coarse FAs with 20–60 min grinding show characteristic behaviour. The third, last stage named the aggregation stage result in the coarsening or stagnation of the median particle size, the decrease or steadying of the surface area values, and changes in the crystalline structure. Regarding the examined FA samples, the 120 min grinding period resulted in a slight increase in the median particle size and surface area compared to 60 min.

The calculated porosities of the FA samples (Table 3) showed an initial increase with longer grinding times but after 10 min a gradual decrease was observed. For narrowly sized particulate matter, the porosity is in a close relationship with the particle size: with decreasing particle size the porosity increases [69]. As the trend in the porosity values and particle size of the examined FAs showed dissimilarities, the explanation for the difference might be another influencing factor, the changed shape of the particles or size ratio of the fine and coarse particles and their respective quantities [70].

Several methods and material properties can be used to assess the pozzolanic activity of materials, such as the strength activity index (also called the pozzolanic activity index) [71–73], Frattini test [74–76], saturated lime test [43,74], or the pozzolanic activity with lime assessing the compressive and flexural strength [72]. These various test procedures often give diverse final values as the examined properties are different, but the relation of the values among one set of experiment serves as an appropriate basis for

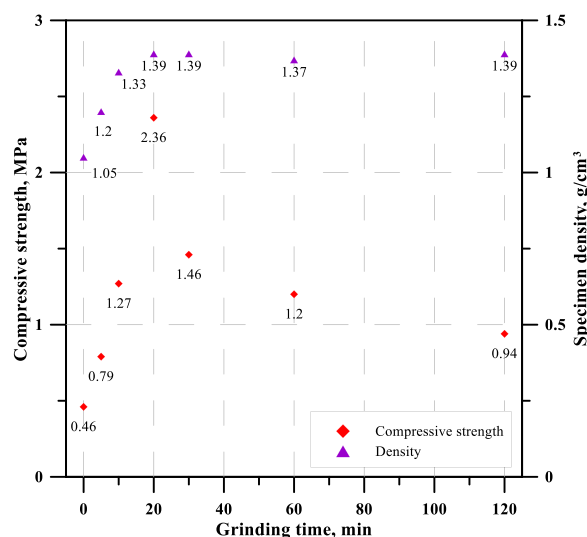


Fig. 10. The changes in the compressive strength and specimen density of geopolymer specimens.

comparison. The pozzolanic activity of FA increases in relation to the higher amount of fine particles in the system, the larger surface area of the bulk and the available Si and Al in the aluminosilicate phases. Thus, pozzolanic activity can also be applied as a method to evaluate the geopolymerization capability of materials, and vice versa, the compressive strength of geopolymers is an appropriate indicator of the pozzolanic activity of the base materials [77,78]. The comparison of the pozzolanic activity of raw, mechanically activated via vibratory milling, ground with ball mill and sieved FAs by Jovanovic et al. (2014) revealed that the mechanical activation of the sample resulted in the highest pozzolanic activity [72]. In the case of the FA samples, around 20–30 min grinding was concluded to be the optimal time to increase the pozzolanic potential of the samples.

Similar results were achieved after the alkali activation of the FA samples, regarding the optimal grinding time. Thus, the use of high-energy mills to mechanically activate FA is a feasible processing option, however, finding the appropriate grinding time for mechanical activation can optimise the material properties and also prevent the application of excessive grinding time and consequently the higher energy consumption. Based on the geopolymer compressive strength values, the 20 min milling time can achieve sufficient strength increase.

The obtained results indicate that even though the application is not widespread, the mechanically activated coarse FA fraction revealed huge potential for the production of cementitious or geopolymer binders, based on the structural changes and the increased reactivity. Even though the achieved geopolymer strength values are low, this can be further increased with the further optimisation of the mixture composition, such as waterglass addition, NaOH molarity change, etc.

5. Conclusions

As part of the research, a lignite-type Class F FA sample was analysed, classified and mechanically activated in a planetary ball mill to investigate the complex utilisation possibility for both FA fractions. Based on the results, the following conclusions can be drawn:

- After classification, the coarse and fine fractions showed considerable composition differences, resulting in the viability of the use of both fractions in various industrial fields, taking advantage of the individual properties of each fraction.
- The geopolymerization of the base and coarse sample revealed the importance of the fine fraction and the optimal component ratios of the mixture.
- The further processing of the coarse fraction via planetary milling resulted in improved material properties, with significantly higher reactivity and possible amorphization of the crystalline structure, providing a promising base material for many industrial applications.
- Examining the geopolymerization potential of the mechanically activated samples, with only 20 min planetary milling, over five times increase in the compressive strength could be achieved.
- Due to the proposed advanced mechanical processing of low-grade fly ash, in accordance with the concept of circular economy, the landfilled amount of FA can be drastically decreased, as the waste material can be used in higher portions as cement supplementary material in construction materials, soil stabilisation, or even for CO₂ sequestration. Additionally, lower CO₂ footprint building material can be produced thanks to the higher recycling ratio after processing.

Declaration of Competing Interest


The authors declare that they have no known competing financial interests or personal relationships that could have appeared to

influence the work reported in this paper.

Data Availability

No data was used for the research described in the article.

Acknowledgements

Supported by the ÚNKP-21–3 New National Excellence Program of the Ministry for Innovation and Technology from the source of the National Research, Development and Innovation Fund.”  The research was partly funded by the Sustainable Development and Technologies National Programme of the Hungarian Academy of Sciences (FFT NP FTA). The authors are grateful to Ferenc Mórícz (Institute of Mineralogy and Geology) for the XRF measurements.

References

- [1] A.D. Kotelnikova, O.B. Rogova, E.A. Karpukhina, et al., Assessment of the structure, composition, and agrochemical properties of fly ash and ash-and-slug waste from coal-fired power plants for their possible use as soil ameliorants, *J. Clean. Prod.* 333 (2022), 130088, <https://doi.org/10.1016/j.jclepro.2021.130088>.
- [2] R. Szabó, Z. Molnár, T. Balogh, R. Mészáros, Development of geopolymer based composite from secondaries, *Epitoanyag - J. Silic. Based Compos. Mater.* 68 (2016) 25–30, <https://doi.org/10.14382/epitoanyag-jsbcm.2016.5>.
- [3] W. Xiang, B. Han, D. Zhou, A. Nzihou, Physicochemical properties and heavy metals leachability of fly ash from coal-fired power plant, *Int. J. Min. Sci. Technol.* 22 (2012) 405–409, <https://doi.org/10.1016/j.ijmst.2011.12.002>.
- [4] T.F. Aquino, S.T. de, Estevam, V.O. Viola, et al., CO₂ adsorption capacity of zeolites synthesized from coal fly ashes, *Fuel* 276 (2020), 118143, <https://doi.org/10.1016/j.fuel.2020.118143>.
- [5] A. Dwivedi, M.K. Jain, Fly ash – waste management and overview: a review, *Recent Res. Sci. Technol.* 6 (2014).
- [6] H. Karami, J. Pooni, D. Robert, et al., Use of secondary additives in fly ash based soil stabilization for soft subgrades, *Transp. Geotech.* 29 (2021), 100585, <https://doi.org/10.1016/j.trgeo.2021.100585>.
- [7] Z. Ma, S. Zhang, H. Zhang, F. Cheng, Novel extraction of valuable metals from circulating fluidized bed-derived high-alumina fly ash by acid–alkali–based alternate method, *J. Clean. Prod.* 230 (2019) 302–313, <https://doi.org/10.1016/j.jclepro.2019.05.113>.
- [8] M. Mostajeran, J.-M. Bondy, N. Reynier, R. Cameron, Mining value from waste: Scandium and rare earth elements selective recovery from coal fly ash leach solutions, *Min. Eng.* 173 (2021), 107091, <https://doi.org/10.1016/j.mineng.2021.107091>.
- [9] D.K. Rajak, A. Raj, C. Guria, A.K. Pathak, Grinding of Class-F fly ash using planetary ball mill: a simulation study to determine the breakage kinetics by direct- and back-calculation method, *South Afr. J. Chem. Eng.* 24 (2017) 135–147, <https://doi.org/10.1016/j.sajce.2017.08.002>.
- [10] C. Wang, G. Xu, X. Gu, et al., High value-added applications of coal fly ash in the form of porous materials: a review, *Ceram. Int.* 47 (2021) 22302–22315, <https://doi.org/10.1016/j.ceramint.2021.05.070>.
- [11] H. Goudarzi, S. Baghshahi, PZT ceramics prepared through a combined method of B-site precursor and wet mechanically activated calcinate in a planetary ball mill, *Ceram. Int.* 43 (2017) 3873–3878, <https://doi.org/10.1016/j.ceramint.2016.12.050>.
- [12] P.L. Guzzo, A.A.A. Tino, J.B. Santos, The onset of particle agglomeration during the dry ultrafine grinding of limestone in a planetary ball mill, *Powder Technol.* 284 (2015) 122–129, <https://doi.org/10.1016/j.powtec.2015.06.050>.
- [13] Y. Nakashima, H. Razavi-Khosroshahi, H. Ishida, et al., Non-firing ceramics: activation of silica powder surface by a planetary ball milling, *Adv. Powder Technol.* 30 (2019) 461–465, <https://doi.org/10.1016/j.apt.2018.11.025>.
- [14] L.P. Turner, B.H. Kueper, K.M. Jaansalu, et al., Mechanochemical remediation of perfluorooctanesulfonic acid (PFOS) and perfluorooctanoic acid (PFOA) amended sand and aqueous film-forming foam (AFFF) impacted soil by planetary ball milling, *Sci. Total Environ.* 765 (2021), 142722, <https://doi.org/10.1016/j.scitotenv.2020.142722>.
- [15] A.G. Patil, S. Anandhan, Influence of planetary ball milling parameters on the mechano-chemical activation of fly ash, *Powder Technol.* 281 (2015) 151–158, <https://doi.org/10.1016/j.powtec.2015.04.078>.
- [16] P. Chindapasrit, S. Homwuttiwong, V. Sirivatnanon, Influence of fly ash fineness on strength, drying shrinkage and sulfate resistance of blended cement mortar, *Cem. Concr. Res.* 34 (2004) 1087–1092, <https://doi.org/10.1016/j.cemconres.2003.11.021>.
- [17] K. Erdogdu, P. Türker, Effects of fly ash particle size on strength of Portland cement fly ash mortars, *Cem. Concr. Res.* 28 (1998) 6.
- [18] L. Krishnaraj, P.T. Ravichandran, Investigation on grinding impact of fly ash particles and its characterization analysis in cement mortar composites, *Ain Shams Eng. J.* 10 (2019) 267–274, <https://doi.org/10.1016/j.asej.2019.02.001>.
- [19] G. Mucsi, A review on mechanical activation and mechanical alloying in stirred media mill, *Chem. Eng. Res. Des.* 148 (2019) 460–474, <https://doi.org/10.1016/j.cherd.2019.06.029>.
- [20] S.H. Lee, E. Sakai, M. Daimon, W.K. Bang, Characterization of fly ash directly collected from electrostatic precipitator, *Cem. Concr. Res.* 29 (1999) 1791–1797, [https://doi.org/10.1016/S0008-8846\(99\)00169-6](https://doi.org/10.1016/S0008-8846(99)00169-6).
- [21] G.L. Golewski, Fracture performance of cementitious composites based on quaternary blended cements, *Materials* 15 (2022) 6023, <https://doi.org/10.3390/ma15176023>.
- [22] G.L. Golewski, Combined effect of coal fly ash (CFA) and nanosilica (nS) on the strength parameters and microstructural properties of eco-friendly concrete, *Energies* 16 (2022) 452, <https://doi.org/10.3390/en16010452>.
- [23] D. Das, K. Nijhuma, A.M. Gabriel, et al., Recycling of coal fly ash for fabrication of elongated mullite rod bonded porous SiC ceramic membrane and its application in filtration, *J. Eur. Ceram. Soc.* 40 (2020) 2163–2172, <https://doi.org/10.1016/j.jeurceramsoc.2020.01.034>.
- [24] G. Chen, F. Yang, S. Zhao, et al., Preparation of high-strength porous mullite ceramics and the effect of hollow sphere particle size on microstructure and properties, *Ceram. Int.* 48 (2022) 19367–19374, <https://doi.org/10.1016/j.ceramint.2022.03.231>.
- [25] S.S. Thavamani, T.P. Amaladhas, M.S. AlSalhi, et al., Transition metal complexes of 4-hydroxy-3-methoxybenzaldehyde embedded in fly ash zeolite as catalysts for phenol hydroxylation, *Chemosphere* 289 (2022), 133167, <https://doi.org/10.1016/j.chemosphere.2021.133167>.
- [26] W. Liu, S. Su, K. Xu, et al., CO₂ sequestration by direct gas–solid carbonation of fly ash with steam addition, *J. Clean. Prod.* 178 (2018) 98–107, <https://doi.org/10.1016/j.jclepro.2017.12.281>.
- [27] B.C. Amoni, A.D.L. Freitas, R.A. Bessa, et al., Effect of coal fly ash treatments on synthesis of high-quality zeolite A as a potential additive for warm mix asphalt, *Mater. Chem. Phys.* 275 (2022), 125197, <https://doi.org/10.1016/j.matchemphys.2021.125197>.
- [28] X. Shao, B. Qin, Q. Shi, et al., Study on the sequestration capacity of fly ash on CO₂ and employing the product to prevent spontaneous combustion of coal, *Fuel* 334 (2023), 126378, <https://doi.org/10.1016/j.fuel.2022.126378>.
- [29] W. Rosita, I.M. Bendiyasa, I. Perdana, F. Anggara, Sequential particle-size and magnetic separation for enrichment of rare-earth elements and yttrium in Indonesia coal fly ash, *J. Environ. Chem. Eng.* 8 (2020), 103575, <https://doi.org/10.1016/j.jece.2019.103575>.

- [30] J. Pan, T. Nie, B. Vaziri Hassas, et al., Recovery of rare earth elements from coal fly ash by integrated physical separation and acid leaching, *Chemosphere* 248 (2020), 126112, <https://doi.org/10.1016/j.chemosphere.2020.126112>.
- [31] K. Gao, O.A. Sahraei, M.C. Iliuta, Ni-based catalysts supported on acid/alkali-activated coal fly ash residue for improved glycerol steam reforming, *Appl. Catal. B Environ.* 301 (2022), 120791, <https://doi.org/10.1016/j.apcatb.2021.120791>.
- [32] X. Chen, J. Zhang, M. Lu, et al., Study on the effect of calcium and sulfur content on the properties of fly ash based geopolymer, *Constr. Build. Mater.* 314 (2022), 125650, <https://doi.org/10.1016/j.conbuildmat.2021.125650>.
- [33] P. Nuaklong, A. Wongs, V. Sata, et al., Properties of high-calcium and low-calcium fly ash combination geopolymer mortar containing recycled aggregate, *Heliyon* 5 (2019), e02513, <https://doi.org/10.1016/j.heliyon.2019.e02513>.
- [34] X. Chen, J. Zhang, M. Lu, et al., Study on the effect of calcium and sulfur content on the properties of fly ash based geopolymer, *Constr. Build. Mater.* 314 (2022), 125650, <https://doi.org/10.1016/j.conbuildmat.2021.125650>.
- [35] R. Kunthawatwong, L. Syllsomchanh, S. Pangdaeng, et al., Recycled Non-Biodegradable polyethylene terephthalate waste as fine aggregate in fly ash geopolymer and cement mortars, *Constr. Build. Mater.* 328 (2022), 127084, <https://doi.org/10.1016/j.conbuildmat.2022.127084>.
- [36] J.H.M. Amran, R. Alyousef, H. Alabduljabbar, M. El-Zeadani, Clean production and properties of geopolymer concrete; a review, *J. Clean. Prod.* 251 (2020), 119679, <https://doi.org/10.1016/j.jclepro.2019.119679>.
- [37] J. Davidovits, Geopolymers, *J. Therm. Anal.* 37 (1991) 1633–1656, <https://doi.org/10.1007/bf01912193>.
- [38] P. Kumar, G. Mucsi, F. Kristály, P. Pekker, Mechanical activation of fly ash and its influence on micro and nano-structural behaviour of resulting geopolymers, *Adv. Powder Technol.* 28 (2017) 805–813, <https://doi.org/10.1016/j.appt.2016.11.027>.
- [39] Mucsi G., Molnár Z., Kumar S. (2014) Geopolymerisation of mechanically activated lignite and brown coal fly ash. *Proc 8th Int Conf Mechanochemistry Mech Alloy INCOME 2014* 126:994–998, <https://doi.org/10.12693/APhysPolA.126.994>.
- [40] B.M. Das, K. Sobhan, *Principles of geotechnical engineering*, Eighth edition/SI edition, Cengage Learning, Stamford, CT, 2014.
- [41] Scheetz B.E., Mohebbi M., Rajabipour F. (2015) Reliability of Loss on Ignition (LOI) Test for Determining the Unburned Carbon Content in Fly Ash. In: 2015 World of Coal Ash (WOCA) Conference in Nashville, TN. p 14.
- [42] Fajtli J., Gombkötő I., Mucsi G., et al. (2017) Mechanikai eljárásai praktikum. Miskolci Egyetemi Kiadó, Miskolc.
- [43] S. Donatello, M. Tyrer, C.R. Cheeseman, Comparison of test methods to assess pozzolanic activity, *Cem. Concr. Compos.* 32 (2010) 121–127, <https://doi.org/10.1016/j.cemconcomp.2009.10.008>.
- [44] W. Mozgawa, M. Król, J. Dyzek, J. Deja, Investigation of the coal fly ashes using IR spectroscopy, *Spectrochim. Acta A Mol. Biomol. Spectrosc.* 132 (2014) 889–894, <https://doi.org/10.1016/j.saa.2014.05.052>.
- [45] J.L. Bishop, M.D. Lane, M.D. Dyar, et al., Spectral properties of Ca-sulfates: gypsum, bassanite, and anhydrite, *Am. Miner.* 99 (2014) 2105–2115, <https://doi.org/10.2138/am-2014-4756>.
- [46] M. Criado, A. Fernández-Jiménez, A. Palomo, Alkali activation of fly ash: effect of the SiO₂/Na₂O ratio, *Microporous Mesoporous Mater.* 106 (2007) 180–191, <https://doi.org/10.1016/j.micromeso.2007.02.055>.
- [47] A. Jain, S. Chaudhary, R. Gupta, Mechanical and microstructural characterization of fly ash blended self-compacting concrete containing granite waste, *Constr. Build. Mater.* 314 (2022), 125480, <https://doi.org/10.1016/j.conbuildmat.2021.125480>.
- [48] A. Machowska, Z. Kledyrński, I. Wilińska, B. Pacewska, A study of the early hydration processes and properties of fly ash-slag binders, *Bull. Mater. Sci.* 42 (2019) 213, <https://doi.org/10.1007/s12034-019-1886-1>.
- [49] A.C. Cavalcanti Gomes, A. de Vasconcelos Ferraz, L.P.G. da Rocha, Characterization of coal fly ash for use in synthesis of zeolites, *Mater. Sci. Forum* 930 (2018) 578–583, <https://doi.org/10.4028/www.scientific.net/MSF.930.578>.
- [50] F. Goodarzi, H. Sane'i, Plerosphere and its role in reduction of emitted fine fly ash particles from pulverized coal-fired power plants, *Fuel* 88 (2009) 382–386, <https://doi.org/10.1016/j.fuel.2008.08.015>.
- [51] J.C. Jeyageetha, S.P. Kumar, Study of SEM/EDXS and FTIR for fly ash to determine the chemical changes of ash in marine environment, *Int. J. Sci. Res* 5 (2013) 6.
- [52] A.K. Ram, S. Mohanty, State of the art review on physiochemical and engineering characteristics of fly ash and its applications, *Int. J. Coal Sci. Technol.* 9 (2022) 9, <https://doi.org/10.1007/s40789-022-00472-6>.
- [53] N. Bouzoubaâ, M.H. Zhang, A. Bilodeau, V.M. Malhotra, The effect of grinding on the physical properties of fly ashes and a portland cement clinker, *Cem. Concr. Res* 27 (1997) 1861–1874, [https://doi.org/10.1016/S0008-8846\(97\)00194-4](https://doi.org/10.1016/S0008-8846(97)00194-4).
- [54] G.L. Golewski, The role of pozzolanic activity of siliceous fly ash in the formation of the structure of sustainable cementitious composites, *Sustain Chem.* 3 (2022) 520–534, <https://doi.org/10.3390/suschem3040032>.
- [55] G. Mucsi, B. Csöke, *Erőművi pernyék fizikai és kémiai tulajdonságai. Erőmű pernye komplex hasznosítása*, Milagrossa Kft., Miskolc, 2014, pp. 67–80.
- [56] L.C. González, M.A. Loubes, M.P. Tolaba, Incidence of milling energy on dry-milling attributes of rice starch modified by planetary ball milling, *Food Hydrocoll.* 82 (2018) 155–163, <https://doi.org/10.1016/j.foodhyd.2018.03.051>.
- [57] G. Mucsi, S. Kumar, B. Csöke, et al., Control of geopolymer properties by grinding of land filled fly ash, *Int. J. Min. Process* 143 (2015) 50–58, <https://doi.org/10.1016/j.minpro.2015.08.010>.
- [58] J. Zhang, Q. Feng, The making of Class C fly ash as high-strength precast construction material through geopolymerization, *Min. Met. Explor.* 37 (2020) 1603–1616, <https://doi.org/10.1007/s42461-020-00283-w>.
- [59] J.N. Yankwa Djobo, A. Elimbi, H.K. Tchakouté, S. Kumar, Mechanical activation of volcanic ash for geopolymer synthesis: effect on reaction kinetics, gel characteristics, physical and mechanical properties, *RSC Adv.* 6 (2016) 39106–39117, <https://doi.org/10.1039/C6RA03667H>.
- [60] W. Liao, H. Ma, H. Sun, et al., Potential large-volume beneficial use of low-grade fly ash in magnesia-phosphate cement based materials, *Fuel* 209 (2017) 490–497, <https://doi.org/10.1016/j.fuel.2017.08.028>.
- [61] Z. Zimar, D. Robert, A. Zhou, et al., Application of coal fly ash in pavement subgrade stabilisation: a review, *J. Environ. Manag.* 312 (2022), 114926, <https://doi.org/10.1016/j.jenvman.2022.114926>.
- [62] K. Ojha, N.C. Pradhan, A.N. Samanta, Zeolite from fly ash: synthesis and characterization, *Bull. Mater. Sci.* 27 (2004) 555–564, <https://doi.org/10.1007/BF02707285>.
- [63] A. Rizzuti, M.C. Dipalo, I. Allegretta, et al., Microwave-assisted solvothermal synthesis of Fe₃O₄/CeO₂ nanocomposites and their catalytic activity in the imine formation from benzyl alcohol and aniline, *Fresenius Environ. Bull.* 10 (2020) 1325, <https://doi.org/10.3390/catal10111325>.
- [64] N.L. Ukwattage, P.G. Ranjith, S.H. Wang, Investigation of the potential of coal combustion fly ash for mineral sequestration of CO₂ by accelerated carbonation, *Energy* 52 (2013) 230–236, <https://doi.org/10.1016/j.energy.2012.12.048>.
- [65] P.L. Guzzo, F.B. Marinho de Barros, B.R. Soares, J.B. Santos, Evaluation of particle size reduction and agglomeration in dry grinding of natural quartz in a planetary ball mill, *Powder Technol.* 368 (2020) 149–159, <https://doi.org/10.1016/j.powtec.2020.04.052>.
- [66] P. Paaver, P. Paiste, M. Liira, K. Kirsimäe, Mechanical activation of the Ca-rich circulating fluidized bed combustion fly ash: development of an alternative binder system, *Minerals* (2021) 11, <https://doi.org/10.3390/min11010003>.
- [67] Wahyudi A., Nurasi T., Rochani S. (2012) Preparation of Nanoparticle Silica from Silica Sand and Quartzite by Ultrafine Grinding. In: *Proceedings of International Conference on Chemical and Material Engineering* 2012. p 8.
- [68] L. Opoczky, Fine grinding and agglomeration of silicates, *Powder Technol.* 17 (1977) 1–7, [https://doi.org/10.1016/0032-5910\(77\)85037-7](https://doi.org/10.1016/0032-5910(77)85037-7).
- [69] S. Zhang, *Relationship between Particle Size Distribution and Porosity in Dump Leaching*, University of British Columbia, 2015.
- [70] D.A. Robinson, A. Thomas, S. Reinsch, et al., Analytical modelling of soil porosity and bulk density across the soil organic matter and land-use continuum, *Sci. Rep.* 12 (2022) 7085, <https://doi.org/10.1038/s41598-022-11099-7>.
- [71] L. Gan, H. Wang, X. Li, et al., Strength activity index of air quenched basic oxygen furnace steel slag, *J. Iron Steel Res Int* 22 (2015) 219–225, [https://doi.org/10.1016/S1006-706X\(15\)60033-4](https://doi.org/10.1016/S1006-706X(15)60033-4).

- [72] I. Jovanovic, Lj Andric, M. Bugarin, et al., Improvement of coal fly ash pozzolanic activity by different physical methods, *J. Min. Met. Min.* 50 (2014) 19–25, <https://doi.org/10.5937/JMMA1401019J>.
- [73] C. Patil, M. Manjunath, S. Hosamane, et al., Pozzolonic activity and strength activity index of bagasse ash and fly ash blended cement mortar, *Mater. Today Proc.* 42 (2021) 1456–1461, <https://doi.org/10.1016/j.matpr.2021.01.251>.
- [74] G. Bumanis, L. Vitola, L. Stipniece, et al., Evaluation of Industrial by-products as pozzolans: A road map for use in concrete production, *Case Stud. Constr. Mater.* 13 (2020), e00424, <https://doi.org/10.1016/j.cscm.2020.e00424>.
- [75] A. Khan, M. Ali Sikandar, M. Tariq Bashir, et al., Assessment for utilization of tobacco stem ash as a potential supplementary cementitious material in cement-based composites, *J. Build. Eng.* 53 (2022), 104531, <https://doi.org/10.1016/j.jobbe.2022.104531>.
- [76] H. Yanguatin, J.H. Ramírez, A. Tironi, J.I. Tobón, Effect of thermal treatment on pozzolanic activity of excavated waste clays, *Constr. Build. Mater.* 211 (2019) 814–823, <https://doi.org/10.1016/j.conbuildmat.2019.03.300>.
- [77] Bondar D. (2009) Alkali Activation of Iranian Natural Pozzolans for Producing Geopolymer Cement and Concrete. PhD thesis, University of Sheffield.
- [78] M. Wang, Y. Liu, C. Feng, et al., Pozzolanic activity enhancement of magnesium-rich nickel slag and geopolymer preparation, *J. Mater. Cycles Waste Manag.* 24 (2022) 2598–2607, <https://doi.org/10.1007/s10163-022-01507-5>.